A GPU-Oriented Algorithm Design for Secant-Based Dimensionality Reduction

Henry Kvinge, Elin Farnell, Michael Kirby, and Chris Peterson Department of Mathematics Colorado State University Fort Collins, CO 80523-1874

Abstract—Dimensionality-reduction techniques are a fundamental tool for extracting useful information from highdimensional data sets. Because secant sets encode manifold geometry, they are a useful tool for designing meaningful datareduction algorithms. In one such approach, the goal is to construct a projection that maximally avoids secant directions and hence ensures that distinct data points are not mapped too close together in the reduced space. This type of algorithm is based on a mathematical framework inspired by the constructive proof of Whitney's embedding theorem from differential topology. Computing all (unit) secants for a set of points is by nature computationally expensive, thus opening the door for exploitation of GPU architecture for achieving fast versions of these algorithms. We present a polynomial-time data-reduction algorithm that produces a meaningful low-dimensional representation of a data set by iteratively constructing improved projections within the framework described above. Key to our algorithm design and implementation is the use of GPUs which, among other things, minimizes the computational time required for the calculation of all secant lines. One goal of this report is to share ideas with GPU experts and to discuss a class of mathematical algorithms that may be of interest to the broader GPU community.

I. Introduction

High performance computing architectures and massive data centers have created a modern data challenge. Supercomputers generate data at ever more amazing rates, in extreme cases upwards of 20,000,000 cores processing power and processing speeds approaching 100 petaflops. Also, advances in data acquisition have us in uncharted territory; e.g., the Australian Square Kilometre Array Pathfinder is generating data measured in petabytes per hour.

How does one begin to interrogate data sets of this magnitude? In this paper we propose that one of the first questions one can pose about data is mathematical, i.e., what is the dimension of the data? Are fast dimension estimates of massive data sets feasible? What is the role of high-performance computing and parallel architectures for dimension-estimation algorithms? Examining all points, or large subsets of points, to identify optimal representation subspaces appears inherently parallelizable. The dimension question provides a window into the complexity of the data and opportunities for data reduction.

Even the question of monitoring these high-performance computing systems is a challenge. Mathematical models for anomaly detection provide an interesting direction, but these approaches also suffer from the curse of dimensionality [1], [2]. Characterizing the behavior of a 100,000,000 variable

dynamical system requires new modeling strategies. Again, understanding the dimension of the data may provide the first step to making the modeling procedure tractable [3].

The outline of this paper is as follows: in Section II, we discuss our proposal for an algorithm that provides both a meaningful projection for dimensionality reduction and a means of estimating the dimension of a data set. We cover foundational mathematical background in Section III. We present the specifics of the proposed algorithm in Section IV and we demonstrate its use on a synthetic example in Section V. In Section VI, we use the algorithm to estimate the dimension of three data sets: a synthetic data set, a data set of digital images, and a hyperspectral data set. Finally, in Section VII we suggest a modified version of the algorithm for noisy data.

II. OVERVIEW

High-dimensional data sets can be both a computational burden and difficult to analyze. Data-reduction algorithms offer a way to reduce these difficulties by mapping the data set into a lower-dimensional space with the goal of retaining as much information as possible. A classical example of such an algorithm is principal component analysis (PCA). In [3], [4], [5], Broomhead and Kirby developed a new framework for data reduction based on Whitney's embedding theorem, a theorem from differential topology which gives an upper bound on the dimension of Euclidean space required to smoothly embed a compact k-dimensional manifold [6, Section 1.8]. The goal of this framework is to produce projections which not only retain differential structure but also have a well-conditioned inverse (roughly, an inverse for which small changes in the domain produce similarly small changes in the range). This property, not necessarily found for projections obtained from other popular methods such as PCA, means that the projection provides a method to compress and decompress the data without loss of information.

In practice, producing projections for a data set $X \subset \mathbb{R}^n$ into \mathbb{R}^m for m < n within the Whitney reduction framework involves finding projections $P: X \subset \mathbb{R}^n \to \mathbb{R}^m$ for which the smallest value of

$$\frac{||P(x_1) - P(x_2)||_{\ell_2}}{||x_1 - x_2||_{\ell_2}}$$

for $x_1, x_2 \in X$ is maximized. This can be more concisely described as follows: let S be the set of all secants of X (that

is, the set of differences of all distinct points in X). Then we seek a projection P that best preserves S. In Section IV of this paper we describe a new algorithm to accomplish this, which we call Secant-Avoidance Projection (SAP).

Because the number of secants for a data set of size n is n(n-1)/2, even relatively small data sets can have large corresponding secant sets. For this reason, the use of GPU architecture is key to the design of this algorithm. Calculation of the secant set itself can be cumbersome on a CPU as the size of n becomes large. Furthermore, many of the steps in the algorithm involve small independent calculations with each secant in S. These can be trivially parallelized and implemented efficiently on a GPU.

We note that our algorithm also provides a method of approximating the dimension of a data set. We outline how this is done in Section VI and provide applications in this context.

III. BACKGROUND THEORY

In this section we discuss some of the background related to the practical question of dimension estimation [7].

A. Topological Dimension

For data sampled from smooth manifolds, e.g, intervals, circles, spheres and tori, the space looks locally flat and it is only at larger scales that the curvature becomes apparent. The dimension of this locally flat space, i.e., the tangent space, is taken to be the dimension of the manifold (which is the same at every point on the manifold). Following [8], we introduce the ϵ -tangent space determined by the singular vectors associated with the singular values of the singular value decomposition (SVD) that scale linearly for small ϵ . It is this subset of the basis elements that determine the tangent space and the topological dimension of the manifold [9].

Theorem 1. [10] The basis vectors whose singular spectrum scales as ϵ for small ϵ form a basis for the tangent space centered at p of an m-dimensional manifold. i.e., those basis vectors for which the set of singular values $\{\sigma_i\}$ of an ϵ -ball centered at p have

$$\sigma_i(p,\epsilon) = k\epsilon + O(\epsilon^2), \quad 1 \le i \le m$$

for some constant k form a basis for the tangent space at p.

It is implicit in the above statement that any basis vector of the local SVD that does not scale linearly lives in a space perpendicular to the tangent space. This is a tractable computation to approximate dimension, especially in low dimensions; see, e.g., [11], [12]. However, in theory it requires the computation of SVDs over many scales at each point on the data set.

B. Whitney's Theorem

A foundational result in differential topology, Whitney's embedding theorem gives an upper bound on the dimension of Euclidean space needed to smoothly embed a finite-dimensional compact differentiable manifold. Recall that an *immersion* is a differentiable function $f: M \to N$ between

two differentiable manifolds M and N, whose derivative is everywhere injective.

Theorem 2. [6] Let M be an m-dimensional differentiable compact manifold. Then there exists an embedding into \mathbb{R}^{2m+1}

The proof of this theorem in [13] uses the construction of the secant set S and argues that the projection has an inverse as long as the point of projection does not lie on or infinitesimally close to any secant line of M.

C. Bi-Lipschitz Criterion

A function f(x) is said to be *bi-Lipschitz* on S if for all $x,y\in S$ it holds that

$$m_1 \|x - y\|_{\ell_2} \le \|f(x) - f(y)\|_{\ell_2} \le m_2 \|x - y\|_{\ell_2}.$$
 (1)

The constants m_1, m_2 can be interpreted as follows:

- m₁ is the injectivity/immersivity parameter and prevents pairs of points from collapsing,
- m₂ is the Lipschitz constant and prevents pairs of points from blowing apart.

The characterization of a function as bi-Lipschitz is connected to dimension estimation [14], [15].

Theorem 3. [16] If a function $f: S \to T$ is bi-Lipschitz, then

$$\dim(S) = \dim(T),$$

where the dimension can be taken as the topological dimension, or the Hausdorff dimension.

Theorem 4. [4] If a function f(x) is bi-Lipschitz, then the inverse function f^{-1} is also bi-Lipschitz with injectivity parameter $1/m_2$ and Lipschitz constant $1/m_1$, i.e.,

$$\frac{1}{m_2} \|x' - y'\|_{\ell_2} \le \|f^{-1}(x') - f^{-1}(y')\|_{\ell_2} \le \frac{1}{m_1} \|x' - y'\|_{\ell_2}.$$

Typically reduction mappings are not optimized for reconstruction and may have ill-conditioned inverses. We note that when f is a projection, the upper bound in (1) is automatically satisfied and only the lower bound needs to be checked.

IV. THE SECANT-AVOIDANCE PROJECTION ALGORITHM

In this section we describe our algorithm for data reduction. Given a data set of k points $X = \{x^{(1)}, \dots, x^{(k)}\} \subset \mathbb{R}^n$ we want to construct a projection $\Pr: \mathbb{R}^n \to \mathbb{R}^m$ such that the distances between points in X are preserved. To accomplish this, we propose, for all pairs $x^{(i)}, x^{(j)} \in X$, to calculate and store the corresponding normalized secant

$$s := \frac{x^{(i)} - x^{(j)}}{||x^{(i)} - x^{(j)}||_{\ell_2}}.$$

Note that we normalize each of these secants so that when we compare their projections, those corresponding to close points and far points are on an equal footing. The calculation of all secants for a data set is trivially parallelizable and is an ideal task for a GPU.

We store secants as the columns of an $n \times p$ matrix S and for iteration i of our algorithm we realize our current projection $Pr^{(i)}$ via an $n \times m$ matrix $P^{(i)}$ whose columns are orthonormal vectors spanning an m-dimensional subspace $M \subset \mathbb{R}^n$. We write these column vectors as $p_1^{(i)}, p_2^{(i)}, \dots, p_m^{(i)}$, and $P^{(i)} =$ $p_1^{(i)} \mid p_2^{(i)} \mid \cdots \mid p_m^{(i)}$. The projection $Pr^{(i)}(s)$ of secant s can then be computed as $P^{(i)T}$ s. Our algorithm is designed to solve the optimization problem

$$P^* = \operatorname*{arg\,max}_{P} \left(\min_{s \in S} ||P^T s||_{\ell_2} \right)$$

where the maximum is taken over all projections P from \mathbb{R}^n to an m-dimensional subspace.

As our initial projection we choose $P^{(1)}=[p_1^{(1)}\mid p_2^{(1)}\mid \cdots\mid p_m^{(1)}]$ to be the first m columns of U, where $S=U\Sigma V^T$ is the singular value decomposition of S. In other words, $Pr^{(1)}$ is the projection given by PCA.

After initializing $P^{(1)}$, the algorithm proceeds as follows: at each iteration i we calculate the ℓ_2 -norms of all secants under the current projection. In other words we find the column of $P^{(i)}^T S$ with the smallest ℓ_2 norm; call this column index j^* . The column index j^* corresponds to the index of the secant s_{i^*} as a column in S that is least well preserved by $Pr^{(i)}$.

We construct $P^{(i+1)}$ from $P^{(i)}$ by rotating $P^{(i)}$ by a small amount toward the direction specified by the secant s_{j^*} . In order to shift $P^{(i)}$ toward this secant we first calculate the projection of this secant $P^{(i)}P^{(i)}$ s_{i^*} in \mathbb{R}^n . Let $p_t^{(i)}$ be the vector from $p_1^{(i)}, \ldots, p_m^{(i)}$ which maximizes $|\langle p_k^{(i)}, s_{j^*} \rangle|$. If all these quantities are zero then we pick $p_t^{(i)} = p_1^{(i)}$. After selecting $p_t^{(i)}$, we run the modified $p_t^{(i)} = p_t^{(i)}$. ified Gram-Schmidt algorithm on the m ordered vectors $\left\{P^{(i)}P^{(i)}{}^{T}s_{j^*}, p_1^{(i)}, p_2^{(i)}, \dots, p_{t-1}^{(i)}, p_{t+1}^{(i)}, \dots, p_m^{(i)}\right\}$ to obtain a new set of orthonormal vectors

$$\left\{ \frac{P^{(i)}P^{(i)^{T}}s_{j^{*}}}{\|P^{(i)}P^{(i)^{T}}s_{j^{*}}\|_{\ell_{2}}}, p_{2}^{(i+1)}, p_{3}^{(i+1)}, \dots, p_{m}^{(i+1)} \right\}$$

which has the same span but now necessarily contains the normalized projection of s_{j^*} . We then set $p_1^{(\tilde{i}+1)}$ to be the unit vector in the direction of

$$(1-\alpha)P^{(i)}P^{(i)}^{T}(s_{i^*}) + \alpha(s_{i^*} - P^{(i)}P^{(i)}^{T}(s_{i^*})),$$

where $\alpha \in [0,1]$ is a small constant that controls the amount that our projection shifts at each step. The results presented in this paper were computed using $\alpha = 0.01$, where this value is chosen to ensure that a minor shift is made in each step and to encourage convergence. Experimentally, a value of $\alpha = 0.01$ appears to achieve those goals.

We summarize the Secant-Avoidance Projection algorithm in Algorithm 1. The computational complexity of the SAP algorithm is dominated by the complexity of the SVD and Gram-Schmidt algorithms as well as that of the determination of the secant with the shortest projected norm. A standard implementation approach would result in completion in time $O(n^5)$. However, there are several ways in which one might improve the asymptotic bound. For example, Monte Carlo approaches to the computation of the SVD and smart updates to the lengths of the projected secants stand to improve the time complexity. Such explorations are a topic for future research.

Algorithm 1 Secant-Avoidance Projection

- 1: **inputs** Secant set S, desired dimension of embedding m, max number of steps (Iterations) or alternative stopping criterion, and shift parameter α .
- 2: Initialize $P^{(1)}$ to be the matrix formed by the first mcolumns of U, where $S = U\Sigma V^T$.
- 3: **for** i < Iterations **do**

- Set $s_{j^*} = \arg\min_{s \in S} ||(P^{(i)})^T s||_{\ell_2}$. Set $p_t^{(i)} = \arg\max_{1 \leq k \leq m} |\langle p_k^{(i)}, s_{j^*} \rangle|$. Apply the modified Gram-Schmidt algorithm to $P^{(i)}P^{(i)}^T s_{j^*}, p_1, \dots, p_{t-1}, p_{t+1}, \dots, p_m$ to obtain a new orthonormal basis

$$\frac{P^{(i)}P^{(i)^T}s_{j^*}}{\|P^{(i)}P^{(i)^T}s_{j^*}\|_{\ell_2}}, p_2^{(i+1)}, \dots, p_m^{(i+1)}.$$

Set $p_1^{(i+1)}$ to be the unit vector in the direction of

$$(1-\alpha)P^{(i)}P^{(i)^{T}}(s_{j^{*}}) + \alpha(s_{j^{*}} - P^{(i)}P^{(i)^{T}}(s_{j^{*}})).$$

- $i+1 \leftarrow i$
- 9: end for
- 10: **return** $Pr^{(i)}$

V. A SYNTHETIC EXAMPLE: TRIGONOMETRIC MOMENT

In this section we show an example of an application of the SAP algorithm and we compare the results to other common projection methods. We construct a synthetic data set by sampling points from the trigonometric moment curve $\phi: \mathbb{R} \to \mathbb{R}^{10}$ defined by

$$\phi(t) := (\cos(t), \sin(t), \cos(2t), \dots, \cos(5t), \sin(5t)).$$

For this example and all following examples, we use a program written in CUDA 8.0 [17]. On two Nvidia Tesla K80 graphics processing units, we

- · construct the secant set for the relevant data set,
- calculate the singular value decomposition for the matrix of all normalized secant vectors using the cuSolver library [18].
- run the algorithm for 100 iterations. For some of the following examples we fix a dimension, and for others, we repeat for various projection dimensions.

Figure 1 shows a projection of the sampled trigonometric moment curve data onto the first three coordinates in \mathbb{R}^{10} . Figure 2 shows the projection into \mathbb{R}^3 obtained from PCA (i.e. the projection of the data from \mathbb{R}^{10} to \mathbb{R}^3 via $Pr^{(1)}$), and Figure 3 shows the projection onto \mathbb{R}^3 obtained from 100 iterations of the Secant-Avoidance Projection algorithm. In each case, we drew 12,800 values from a uniform random distribution

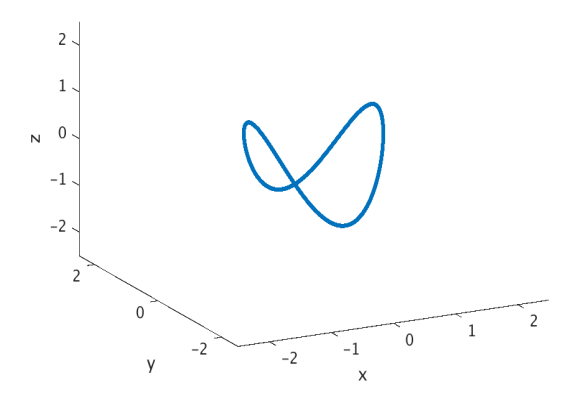


Fig. 1: The projection of the function ϕ onto the first three coordinate directions in \mathbb{R}^{10} . Clearly, much information is lost by ignoring the content in the remaining 7 coordinates. Compare to the projections into \mathbb{R}^3 provided by PCA, which maximizes variance, and to SAP, which seeks a projection with a smooth inverse (Figures 2 and 3, respectively).

Projection of Trigonometric Moment Curve (PCA)

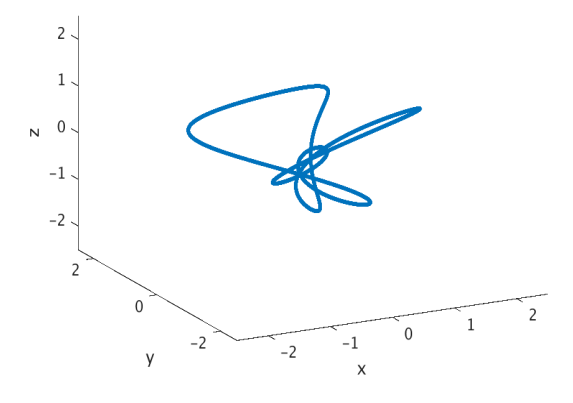


Fig. 2: The projection of the function ϕ into \mathbb{R}^3 via PCA. Recall that the projection provided by PCA is the projection that captures maximal variance in the data.

on $[0,2\pi]$ to get a sampling of points on the trigonometric moment curve.

Qualitatively, as seen in Figures 1, 2, and 3, the three methods of constructing projections have captured different aspects of the data set through their projections into \mathbb{R}^3 . From the perspective of the norm of the shortest projected secant, we find that SAP outperforms both the naïve projection and the PCA projection: the norms of the shortest projected secants, in order, are $0.1013,\ 0.0466,\$ and $0.1677.\$ It is worth noting that PCA and SAP are methods of projection defined in terms of particular optimization problems. So while PCA, by construction, will maximize variance, SAP aims to maximize the norm of the shortest projected secant. We see in this example that SAP has indeed outperformed PCA with respect

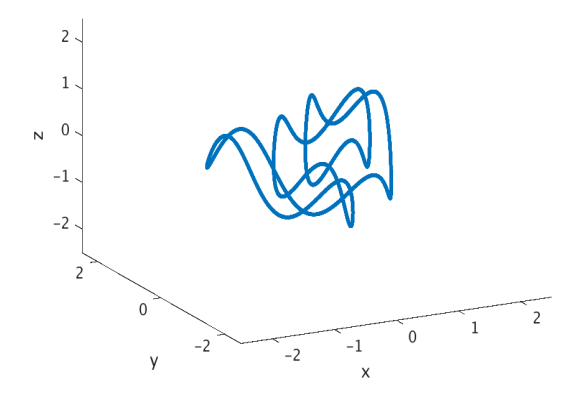


Fig. 3: The projection of the function ϕ into \mathbb{R}^3 via SAP. Recall that SAP seeks to produce a projection that maximizes the minimum projected norm across all secants in the data set.

to this metric, as it is designed to do.

VI. APPROXIMATING THE DIMENSION OF A DATA SET

A. A synthetic example

Even in the case where one is not interested in finding a specific projection, the SAP algorithm can be used to better understand the nature of the data. Specifically, it can give a good sense of the dimensionality of the data. One way to observe this is to run the algorithm for a range of different projection dimensions. One should see the norm of the shortest secant for each projection begin to dramatically increase as the projection dimension increases. Via Whitney's theorem, the dimension at which this occurs leads to a good approximation of the dimension of the data.

As a synthetic example we sampled 256 points uniformly from each of the following smooth manifolds:

1) the curve $f: \mathbb{R} \to \mathbb{R}^3$

$$f(t) = (\cos(t), \sin(t), \cos(2t))$$

smoothly embedded into \mathbb{R}^{15} ,

- 2) a 2-dimensional torus from \mathbb{R}^3 smoothly embedded into \mathbb{R}^{15} .
- 3) a 3-dimensional sphere from \mathbb{R}^4 smoothly embedded into \mathbb{R}^{15} .

According to Whitney's embedding theorem, we expect that the maximum dimension required to embed the curve, torus, and sphere is 3, 5, and 7, respectively. In Figure 4, we see that the SAP algorithm provides an embedding for the three data sets in Euclidean space at these respective dimensions. Specifically, the norm of the shortest projected secant has increased away from zero for these dimensions. We note further that the SAP algorithm provides embeddings at dimensions below the Whitney upper bounds in the case of the torus and 3-sphere. While it is not uncommon for embeddings to exist in dimensions below the Whitney upper bound, the appearance of such embeddings here further highlights the

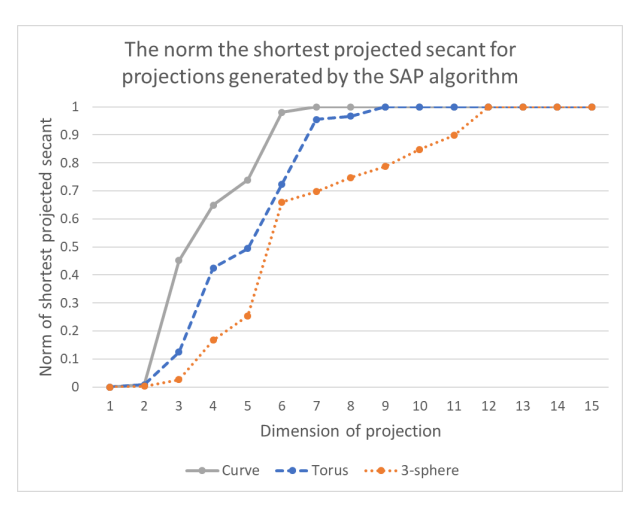


Fig. 4: The ℓ_2 -norm of the shortest secant projection as a function of the dimension of the projection. Note that the dimensions at which the data sets appear to have successful embeddings agree with those provided as upper bounds by Whitney's embedding theorem (3, 5, and 7, respectively). Also note that the results reflect the relative dimensionality of the data sets.

potential usefulness of the SAP algorithm for dimensionality reduction. We observe as well that there is a qualitative distinction between the behavior of the three data sets shown in Figure 4. The norm of the shortest projected secant vector for the three data sets preserves the relative dimensionality relationships between the data sets.

B. The pumpkin illumination space

We demonstrate the use of our algorithm on an illumination space data set. We collected the data for use in the Pattern Analysis Lab at Colorado State University. The data consists of images of a solid object under varying illumination conditions. Specifically, we capture images of a plastic Halloween jack-olantern under varying illumination conditions. The images are color images of size 480×720 . We pre-process by using PCA to reduce dimension and remove noise. Consequently, we have a set of 200 data points in \mathbb{R}^{200} , each of which corresponds to one of the original images.

This data set illustrates the potential value of the Secant-Avoidance Projection algorithm. The data set represents a sample of a subspace of the illumination space of the pumpkin, analogous to many existing data sets that capture individuals and objects under varying illumination. Illumination spaces of people have been well-studied and there have been attempts to understand the dimension of such spaces; see, e.g., [19], [20], [21], [22]. We conjecture that the illumination space of the pumpkin will have similar characteristics, and the SAP algorithm provides a means of understanding the dimensionality of the sampled subspace of the illumination space (we expect to see a subspace because the variations in illumination were restricted to a subset of those that would provide a broad representation of the set of all possible illuminations).

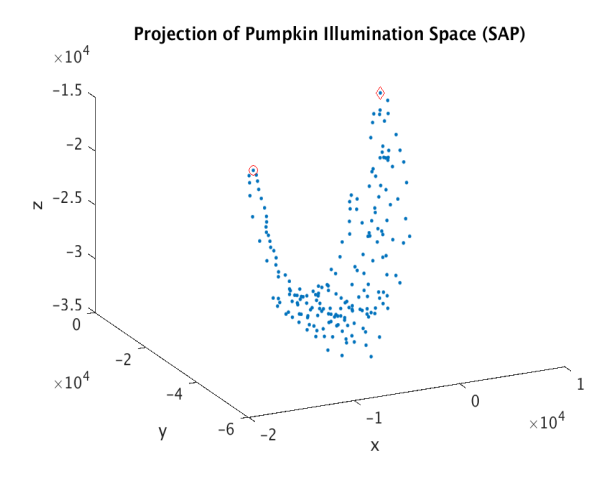


Fig. 5: The projection of the pumpkin data set using the SAP algorithm. Two distinguished points are marked with a red circle and a red diamond - see Figure 7 for the corresponding images from the original pumpkin illumination space data set.

Projection of Pumpkin Illumination Space (SAP)

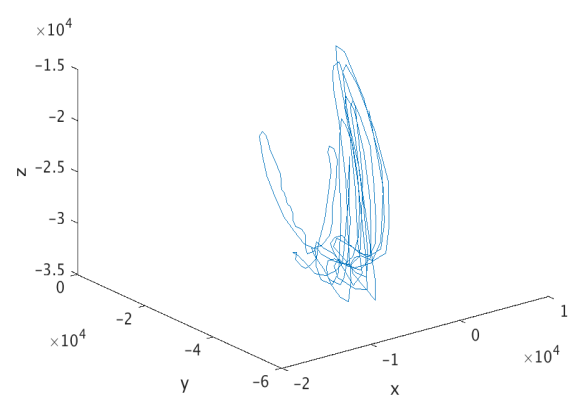


Fig. 6: The projection of the pumpkin data set using the SAP algorithm with points connected by their order in the time series in which the data was collected.

The pumpkin illumination space data is a real-world data set with noise and unknown structure, and we do not know *a priori* the natural dimension of the data. But dimensionality, in general, is of primary importance for making data storage and analysis a manageable task. By applying the SAP algorithm, we obtain an estimate of the dimension of this data set. In this case, we note that the SAP algorithm provides a diffeomorphic copy of the data in \mathbb{R}^3 . Using Whitney's Theorem, we speculate that the subspace of the illumination space determined by these constrained lighting conditions has dimension one.

We can further understand characteristics of the data set that become apparent after applying the SAP projection. For example, note that two points in the projection shown in Figure 5 appear to be extrema; by viewing the images from the original data set that correspond to those extremal points, we note that indeed, we have found points that correspond to



Fig. 7: Images Corresponding to Extremal Points in Projection to \mathbb{R}^3 via SAP. The left image corresponds to the red circle and the right image corresponds to the red diamond in Figure 5.

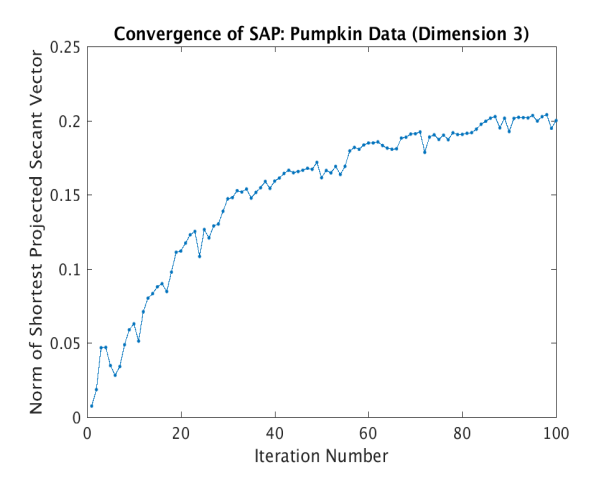


Fig. 8: The convergence of the SAP algorithm on the pumpkin data set. The norm of the shortest projected secant vector generally increases with iteration number.

extreme lighting conditions (Figure 7). Qualitatively, the SAP projection appears to have preserved fundamental features in the data set. For example, the data set can be viewed as a time series as a consequence of the way the data was captured - each successive data point corresponds to a small change in lighting conditions. Thus, we would hope that a good projection would preserve this feature of the data, and indeed, if one connects the points in the time series as in Figure 6, we see that the smooth light variations that varied repeatedly from one extreme to another resulted in an embedding that parametrizes a non-self-intersecting path in three-space.

In Figure 8, we see the convergence of the algorithm over 100 iterations, where the dimension has been fixed to be three. Note that while there are small perturbations, the norm of the shortest projected secant vector increases with the iteration number and thus we expect that the projections are getting correspondingly better.

We compare the performance of the SAP algorithm against that of PCA in Figure 9. Note that both would provide relatively good projections into \mathbb{R}^{20} , but the SAP algorithm outperforms PCA significantly at lower dimensions and per-

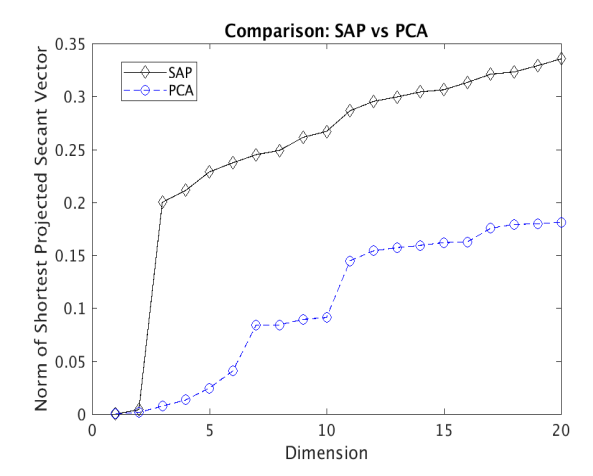


Fig. 9: Comparison of the norm of the shortest projected secant vector as a function of dimension after computing a projection using PCA and a projection using SAP on the pumpkin data set. Note that the SAP algorithm outperforms PCA at lower dimensions and persists through high dimensions according to this measure of success.

sists in providing a better projection for higher dimensions as well (with respect to this measure of success). Further, the manner of construction of the data set suggests that the data should live on a one-dimensional manifold and hence, the embedding into \mathbb{R}^3 by the SAP algorithm is consistent with the upper bound from Whitney's Theorem.

C. Indian Pines hyperspectral data cube

As our final example we consider the application of our algorithm to a modified version of the Indian Pines hyperspectral data set (some bands covering the region of water absorption are removed) [23]. The data cube is $145 \times 145 \times 200$; that is, there are 200 bands, each with spatial resolution of 145×145 . We define a data set $X \subset \mathbb{R}^{200}$ to be the collection of vectors of spectral information taken across all pixel locations. We then have |X| = 21,025. The number of secants associated to this number of points is too massive to handle with the current version of the SAP algorithm so we use a sampling technique and show that in this example at least, such a strategy yields similar results across different random samples.

In Figure 10 we show the plot of the dimension of the projection versus the norm of the shortest projected secant for ten experiments in which we randomly sample 512 points from X and run the SAP algorithm on the associated secant set. As can be seen, aside from minor deviations, these curves are all very similar suggesting that sampling points might be a reasonable strategy to adopt in the setting when the total number of secants in the data set is very large. Note also that in all cases the curve jumps from less than 0.05 to 0.2 as the projection dimension increases from 3 to 4. Thus, we have an embedding of the Indian Pines data into Euclidean space of dimension 4. If the data resides on a manifold, that manifold most likely has dimension two.

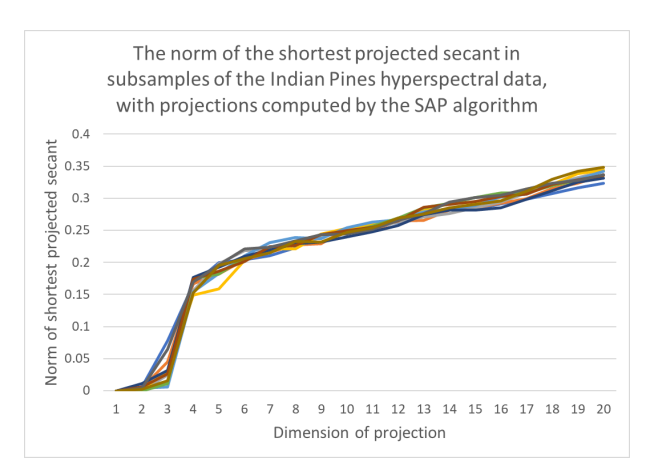


Fig. 10: The ℓ_2 -norm of the shortest secant projection as a function of the dimension of the projection for the Indian Pines data set. Each curve in the graph corresponds to SAP-algorithm projections computed for a subsample of 512 points from the Indian Pines data set. Note the sudden jump in ℓ_2 -norm when the dimension of the projection increases to 4.

VII. DATA WITH NOISE

In the real world, data is almost always contaminated with some amount of noise. If a data set in \mathbb{R}^n sits on an m-dimensional manifold M with m < n, then adding noise will tend to push data points off of M, thereby increasing its apparent dimension. Since we are usually more interested in calculating the dimension of the pure signal without noise, it is useful to develop tests of dimensionality which are resistant to added noise. In this section we suggest an adaptation to the SAP algorithm for use on noisy data.

The idea behind this adaptation stems from the simple observation that when noise is added to a data set it perturbs the positions of points. We therefore expect that the direction of secants between points which are close together will change much more than the direction of secants between points which are far apart. In fact, we can imagine that if two points are sufficiently close, then when noise is added, their secant could be rotated to any direction.

We propose to adapt the SAP algorithm for the setting of noisy data by including an additional step in which secants are thresholded by length. That is, prior to normalization, we discard any secants with length less than some predetermined threshold ℓ . This thresholding value ℓ is then an additional parameter to the algorithm. There is a clear trade-off in potential choices of the size of ℓ : a small ℓ may lead to noise-based structure persisting in the data, and a large ℓ may cause small-scale structure in the data to be lost.

In Figure 11 we show the result of adding random Gaussian noise to points drawn from the trigonometric moment curve $\phi: \mathbb{R} \to \mathbb{R}^{10}$ from Section V; the noise is added independently in each coordinate and has mean 0 and standard deviation 0.1. Figure 12 shows the result of running the SAP algorithm on the data without any noise added, with the noise added but without thresholding, and with the noise added and

Projection of Noisy Trig. Moment Curve onto First 3 Coordinates

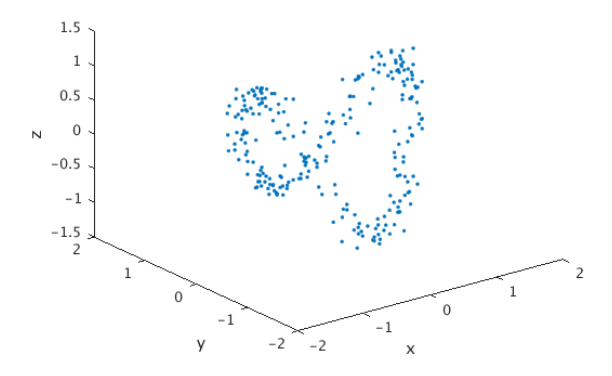


Fig. 11: Projection of Trigonometric Moment Curve with noise onto first three coordinate directions. The noise is independent for each coordinate and has mean 0 and standard deviation 0.1.

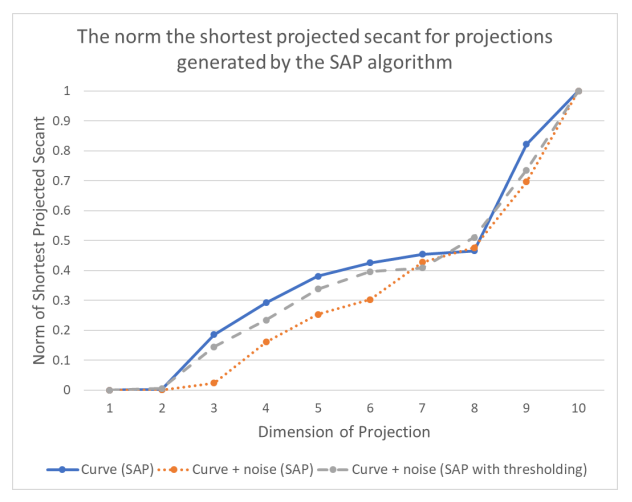


Fig. 12: We compare the norm of the shortest projected secant for: 1) SAP applied to points sampled from the curve defined by ϕ from Section V, 2) SAP applied to ϕ with noise added, and 3) SAP with thresholding applied to ϕ with noise added. Note that the thresholding procedure has improved the embedding and made the results more similar to the no-noise setting.

thresholding secants at length 2. Note that the thresholding procedure has improved the norm of the shortest projected secant of the noisy data to be more similar to the setting in which there is no noise. This is notably the case for projections of dimensions 3-6, which is where we would look to better understand the dimension of this data set. In fact, comparing Figure 12 to Figure 4, we note that the plot of ϕ with noise and no thresholding looks similar to the plot of a genuinely higher dimensional data set. Thresholding secants removes this ambiguity.

VIII. CONCLUSION

In this paper we described a novel algorithm for dimensionality reduction. The Secant-Avoidance Projection algorithm produces projections of the data into a lower-dimensional space. Importantly, these projections preserve dimension and have smooth inverse. Since our algorithm requires many independent calculations with the elements of the secant set, it is well-suited to a GPU implementation. We also show that besides finding good projections of a data set, our algorithm can be used to identify the approximate dimension of a data set.

There remain several related open questions and directions for future work; we highlight a selection here.

- 1) We have proposed a variation of the SAP algorithm for noisy data. This variation incorporates a threshold ℓ , where we discard any secants shorter than ℓ . A next step is the development of a rigorous method of determining ℓ for an arbitrary data set.
- 2) GPUs provide an ideal setting for the SAP algorithm because of the natural parallelization of computation of the secant set. Further work should be done to develop an efficient algorithm that utilizes GPUs to their full extent throughout the implementation.
- 3) We recognize that the advantages gained by parallel computation of the secant set on the GPU have limitations. One avenue for further research lies in potential means of combining information from repeated sampling from a data set with independent applications of the SAP algorithm. One algorithm we suggest is to cluster resulting projections and to compute an appropriate average for each cluster, resulting in several potentially useful methods of projection. Such an algorithm would be particularly useful in the setting in which the memory required for computation of the full secant set is infeasible.
- 4) The proposed algorithm provides no guarantees of convergence to a global optimum. Extensions of this work could propose sufficient conditions for global extrema or an algorithm that does have such a guarantee.

With high-dimensional data being generated at an unprecedented rate, we can expect that demand will only increase for methods of (i) deducing the actual dimension of data and (ii) reducing the dimension of data. Ultimately, we hope that this paper will serve as a first step toward a broader conversation on how to best harness the power of GPU computing to develop secant-based methods that offer efficient solutions to these problems.

ACKNOWLEDGEMENTS

This paper is based on research partially supported by the National Science Foundation under Grants No. DMS-1513633, and DMS-1322508 as well as DARPA awards N66001-17-2-4020 and D17AP00004.

REFERENCES

- [1] Joshua Thompson, David W. Dreisigmeyer, Terry Jones, Michael Kirby, and Joshua Ladd, "Accurate fault prediction of BlueGene/P RAS logs via geometric reduction," in *Proceedings 1st Workshop on Fault-Tolerance for HPC at Extreme Scale (FTXS 2010)*, Chicago, Illinois, 2010.
- [2] Kun Wang, Josh Thompson, Chris Peterson, and Michael Kirby, "Identity maps and their extensions on parameter spaces: Applications to anomaly detection in video," in *Science and Information Conference* (SAI), 2015. IEEE, 2015, pp. 345–351.
- [3] D.S. Broomhead and M. Kirby, "Large dimensionality reduction using secant-based projection methods: The induced dynamics in projected systems," Nonlinear Dynamics (Special Issue on Reduced Order Modelling), vol. 41, no. 1-3, pp. 47–67, 2005.
- [4] D.S. Broomhead and M. Kirby, "A new approach for dimensionality reduction: Theory and algorithms," SIAM J. of Applied Mathematics, vol. 60, no. 6, pp. 2114–2142, 2000.
- [5] D.S. Broomhead and M. Kirby, "The Whitney reduction network: a method for computing autoassociative graphs," *Neural Computation*, vol. 13, pp. 2595–2616, 2001.
- [6] Victor Guillemin and Alan Pollack, Differential topology, AMS Chelsea Publishing, Providence, RI, 2010, Reprint of the 1974 original.
- [7] W. Hurewicz and H. Wallman, *Dimension theory*, Princeton mathematical series. Princeton University Press, 1948.
- [8] D. S. Broomhead, R. Jones, and G. P. King, "Topological dimension and local coordinates from time series data," J. Phys. A: Math. Gen, vol. 20, pp. L563–L569, 1987.
- [9] James R. Munkres, *Topology: a first course*, Prentice Hall, Englewood Cliffs, N.J., 1975.
- [10] DS Broomhead, R Indik, AC Newell, and DA Rand, "Local adaptive Galerkin bases for large-dimensional dynamical systems," *Nonlinearity*, vol. 4, no. 2, pp. 159, 1991.
- [11] R.V. Abadi, D. S. Broomhead, R.A. Clement, J.P. Whittle, and R. Worfolk, "Dynamical systems analysis: A new method of analysing congenital nystagmus waveforms," Technical Report 97-3, UMIST Applied Mathematics, 1997.
- [12] D. Hundley and M. Kirby, "Estimation of topological dimension," in *Proceedings of the Third SIAM International Conference on Data Mining*, San Fransico, 2001, pp. 194–202.
- [13] Morris W. Hirsch, Differential topology, vol. 33 of Graduate Texts in Mathematics, Springer-Verlag, New York, 1994, Corrected reprint of the 1976 original.
- [14] M. Anderle, D. Hundley, and M. Kirby, "The bilipschitz criterion for mapping design in data analysis," *Intelligent Data Analysis*, vol. 6, no. 1, pp. 85–104, 2002.
- [15] M. Kirby, Geometric Data Analysis: An Empirical Approach to Dimensionality Reduction and the Study of Patterns, Wiley, 2001.
- [16] Kenneth Falconer, Fractal geometry, John Wiley & Sons, Inc., Hoboken, NJ, second edition, 2003, Mathematical foundations and applications.
- [17] John Nickolls, Ian Buck, Michael Garland, and Kevin Skadron, "Scalable parallel programming with CUDA," *Queue*, vol. 6, no. 2, pp. 40–53, Mar. 2008.
- [18] NVIDIA, "Cusolver library," 2018, [Online; accessed 25-February-20181.
- [19] Peter N Belhumeur and David J Kriegman, "What is the set of images of an object under all possible illumination conditions?," *International Journal of Computer Vision*, vol. 28, no. 3, pp. 245–260, 1998.
- [20] Athinodoros S. Georghiades, Peter N. Belhumeur, and David J. Kriegman, "From few to many: Illumination cone models for face recognition under variable lighting and pose," *IEEE transactions on pattern analysis and machine intelligence*, vol. 23, no. 6, pp. 643–660, 2001.
- [21] Jen-Mei Chang, Michael Kirby, Holger Kley, Chris Peterson, Bruce Draper, and J Ross Beveridge, "Recognition of digital images of the human face at ultra low resolution via illumination spaces," in Asian Conference on Computer Vision. Springer, 2007, pp. 733–743.
- [22] Jen-Mei Chang, J Ross Beveridge, Bruce A Draper, Michael Kirby, Holger Kley, and Chris Peterson, "Illumination face spaces are idiosyncratic.," IPCV, vol. 2, pp. 390–396, 2006.
- [23] Grupo de Inteligencia Computacional, "Hyperspectral remote sensing scences," 2014, http://www.ehu.eus/ccwintco/index.php/Hyperspectral_ Remote_Sensing_Scenes, Last accessed on 2018-4-30.